Polyhedron 235 (2023) 116350

Contents lists available at ScienceDirect

Polyhedron

journal homepage: www.elsevier.com/locate/poly

# Synthesis, electronic structure and interaction of rhodium(I) and iridium(I) bisimine-acenaphthalene complexes with $CO_2$

Wynand J. Louw [a], Shankara G. Radhakrishnan [a,1,*], Frederick P. Malan [a], Daniela I. Bezuidenhout [b,1,*]

[a] Department of Chemistry, University of Pretoria, Private Bag X20, Hatfield 0028, Pretoria, South Africa
[b] Laboratory of Inorganic Chemistry, Environmental and Chemical Engineering, University of Oulu, P.O. BOX 3000, FI-90014 Oulu, Finland

ARTICLE INFO

*Keywords:*
Rhodium(I)
Iridium(I)
BIAN
Redox non-innocent
$CO_2$ reduction

ABSTRACT

The bis(arylimino)acenaphthalene (BIAN) group of α-diimine compounds has shown promising electron sink behaviour and redox non-innocent activity as ligands to main group and transition metals. Here we present a series of rhodium(I) and iridium(I) complexes of BIAN derivatives with 2,6-diisopropylphenyl (DippBIAN, DB) and 2,4,6-trimethylphenyl (MesBIAN, MB), featuring various electron withdrawing and donating ancillary ligands. The crystal structures of square planar complexes **1b** [RhMB(cod)]$PF_6$, **1d** [IrMB(cod)]$PF_6$, **2a** [RhDB$(CO)_2$]$PF_6$, **2b** [RhMB$(CO)_2$]$PF_6$, **2c** [IrDB$(CO)_2$]$PF_6$ and **3a** [RhDB(CO)$(PEt_3)$]$PF_6$ are reported, as well as the square pyramidal structure of **4c** [IrDB(cod)Cl]. The C-N and C-C bond lengths within the bisimine moiety for the structures of **2a** and **4c** suggest that the DippBIAN ligands are present in a reduced state, however, all other data from our multi-technique analyses correspond to results for neutral BIAN ligands. These contrasting results are indicative of the DippBIAN's non-innocent behaviour, accepting additional electron density from the metal centre due to push–pull mechanism between the ancillary and BIAN ligands. The electrochemical study in non-coordinating solvent $CH_2Cl_2$ revealed that all complexes featured at least one reversible, ligand-centred reduction event at less negative potentials (above –1.0 V vs $Ag/Ag^+$). In addition, preliminary results from our electrocatalytic $CO_2$ reduction study has shown a promising interaction between $CO_2$ and complex **3a**, paving the way for exploring heterogeneous catalysis on these class of compounds

## 1. Introduction

Bis(arylimino)acenaphthalene (BIAN) ligands are a class of α-diimines which have shown promising redox non-innocent properties [1,2]. Metal complexes with BIAN ligands [3–5] initially focused on homogeneous catalysis applications, with emphasis on the alteration of the steric and electronic properties by functionalisation of the aryl imine groups [1,2]. This in turn has led to an extensive library of transition metal complexes featuring various BIAN ligand derivatives. Perhaps the most well-known examples are the Ni-BIAN complexes, the so-called Brookhart catalysts, used in industry for ethylene polymerisation [5–8], while other applications of BIAN complexes have included luminescence properties [9–11]. Investigation of the redox non-innocent behaviour of the BIAN ligands have largely been limited to 3*d* metals (iron, titanium and vanadium) [12–18]. It has been reported that imines are electrochemically active in the presence of $CO_2$ [19], and that $CO_2$ electroreduction occurs as part of an inner sphere electron transfer mechanism [20]. Thus, more recent applications of BIAN ligands have looked into the ever growing field of $CO_2$ reduction, with Re(I)BIAN carbonyl complexes reported which catalysed a two-electron $CO_2$ photocatalytic reduction [21], as well as a Rh(III)BIAN complex which has shown $CO_2$ electrocatalytic reduction ability following its *in situ* reduction to the Rh(I) oxidation state [22,23]. Before these studies, Rh(I)BIAN complexes were reported as part of synthetic [24,25] or catalytic studies [26,27], while reactivity with the solvent acetonitrile complicated electrochemical analyses of the single five-coordinate complex previously reported [22,23].

Expanding our understanding of the electronic structure and redox behaviour of transition metal BIAN complexes will inform further studies into the underlying processes involved in the electrochemical reduction of $CO_2$, which has been observed for this group of compounds [21–23,28]. Herein we report a systematic electrochemical study of a

* Corresponding authors.
*E-mail addresses:* shankara.radhakrishnan@up.ac.za (S.G. Radhakrishnan), daniela.bezuidenhout@oulu.fi (D.I. Bezuidenhout).
[1] Author Footnote.

https://doi.org/10.1016/j.poly.2023.116350
Received 17 January 2023; Accepted 23 February 2023
Available online 28 February 2023

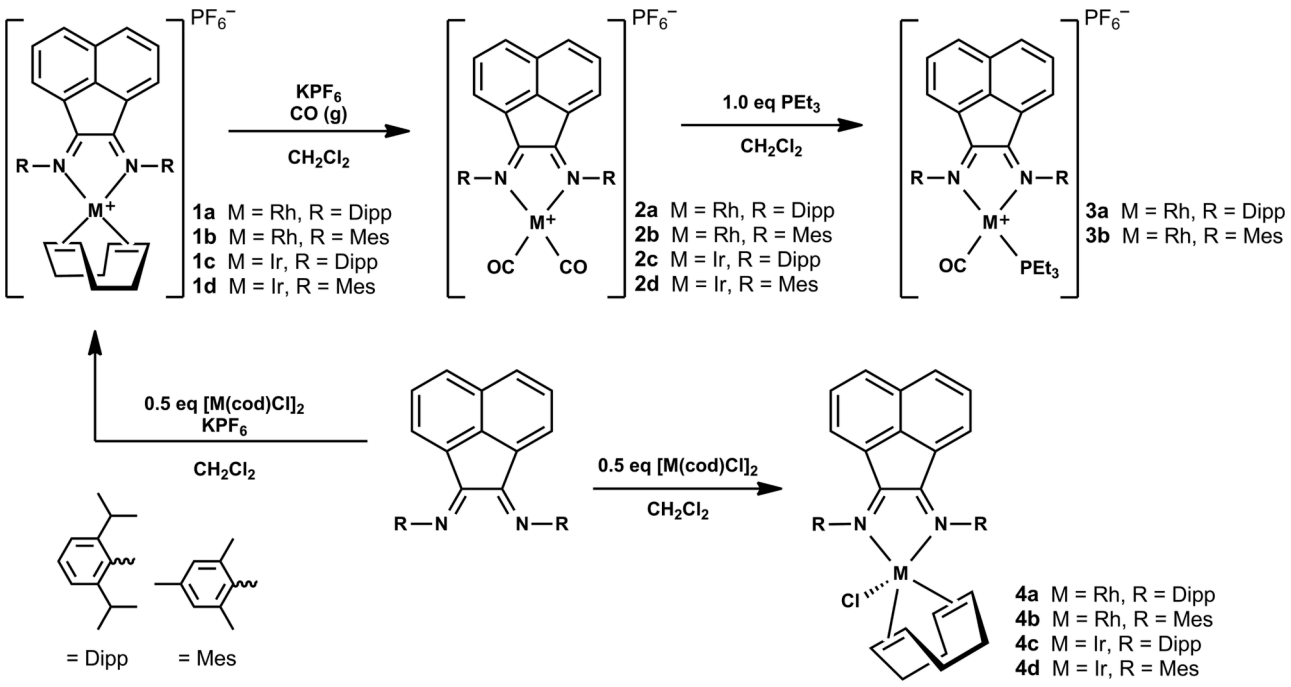


**Scheme 1.** Reaction scheme for the synthesis of reported complexes **1–4**.

series of BIAN complexes of group 9 metals Rh(I) and Ir(I), featuring either 4- or 5-coordinate geometries and a preliminary study of their application in electrochemical $CO_2$ reduction.

The archetypal 1,2-bis[(2,6-diisopropylphenyl)imino]acenaphthalene (DippBIAN, DB) and 1,2-bis[(2,4,6-trimethylphenyl)imino]acenaphthalene (MesBIAN, MB) ligands were chosen for the present work not only for their ease of synthesis in high yields, but also the availability of critically reviewed data of these ligands' physicochemical properties and reactivity with main group, *s*- and *p*-block elements [29], as well as a variety of transition metals which forms a basis in understanding of the present system. Four groups of derivative complexes were investigated featuring ancillary ligands known for exhibiting different degrees of electron withdrawing or donating character in coordination complexes: σ-/π-donor/π-acceptor 1,5-cyclooctadiene (cod), CO and triethylphosphine ($PEt_3$), and π-donating chlorido ligands (Scheme 1).

In an effort to assist in the assignment of the relevant electrochemical events that are directly related to the reduction and oxidation of the original analyte complex, each complex was computationally modelled in eight different oxidation states – representative of the complexes' initial ground state, after losing 1 to 3 electrons, as well as after gaining 1 to 4 electrons. A comparative investigation into the changes between the frontier molecular orbitals (FMOs) of these oxidation states was performed to establish the localisation of observed redox events.

## 2. Experimental

### 2.1. General information

Standard Schlenk line techniques were utilised with $N_2$ atmosphere, unless otherwise specified. All reagents were purchased from Sigma-Aldrich and used without prior purification. The precursor $[Rh(cod)Cl]_2$ [30] and $[Ir(cod)Cl]_2$ [31] dimers were prepared according to published procedures. DippBIAN and MesBIAN ligands were synthesised according to the procedures published by Paulovikova [32] and Gasperini [33] respectively. Nuclear Magnetic Resonance (NMR) spectra were recorded on a Bruker Ultrashield Plus 400 AVANCE 3 or Ultrashield 300 AVANCE 3 spectrometers, at 25 °C, using $CDCl_3$ as solvent. The $^1H$ NMR spectra were recorded at 400.13 or 300.13 MHz, the $^{13}C$ NMR spectra at 100.613 or 75.468 MHz, $^{31}P$ spectra at 162.01 or 121.49 MHz, and $^{19}F$ spectra at 376.57 or 282.40 MHz respectively. All chemical shifts reported are referenced to the residual hydrogen peak of deuterated chloroform ($CDCl_3$) at 7.26 ppm for $\delta_H$, and 77.00 ppm for $\delta_C$. All coupling constants (*J*) are reported in Hz. Spectral coupling patterns as assigned as: **s**–singlet, **d**–doublet, **t**–triplet, **q**–quartet, **quint**–quintet, **sept**–septet, **m**–multiplet, **br**–broad signal. Quaternary carbons that could be definitively identified are labelled as $\mathbf{C_q}$. Solid state infrared transmittance spectra were recorded on a Bruker Alpha II FT-IR spectrometer with the platinum-ATR module (monolithic diamond crystal window). HPLC grade $CH_2Cl_2$ purged with Ar was used for all UV–vis and electrochemical measurements. Full synthesis and characterisation details of complexes **1**–**4** are provided in the supporting information (SI), section S1.

### 2.2. Crystallography

Single crystal diffraction experiments of complexes **1b**, **1d**, and **3a** were analysed using Quazar multi-layer optics monochromated Mo Kα radiation (k = 0.71073 Å) on a Bruker D8 Venture kappa geometry diffractometer with duo IμS sources, a Photon 100 CMOS detector and APEX III control software [34]. Data reduction was performed using SAINT+ [34], and the intensities were corrected for absorption using SADABS-2016 [34]. Single crystal diffraction experiments of complexes **2a**, **2b**, **2c**, and **4c** were performed on a Rigaku XtaLAB Synergy R diffractometer, with a rotating-anode X-ray source and a HyPix CCD detector. Data reduction and absorption were carried out using the CrysAlisPro (version 1.171.40.23a) software package [35]. All X-ray diffraction measurements were performed at 150(1) K, using an Oxford Cryogenics Cryostat. All structures were solved by direct methods with SHELXT-2018 [36] and refined using SHELXL-2018 packages [37]. H atoms were placed in geometrically idealised positions and constrained to ride on their parent atoms. For data collection and refinement parameters, see the SI section S2. The X-ray crystallographic coordinates for the structures of **1b**, **1d**, **2a**, **2b**, **2c**, **3a** and **4c** have been deposited at the Cambridge Crystallographic Data Centre (CCDC), with deposition numbers CCDC 2161246–2161252. The data may be accessed free of charge from The Cambridge Crystallographic Data Centre *via* http

s://www.ccdc.cam.ac.uk/data_request/cif.

### 2.3. Electrochemistry

Electrochemical studies were carried out on a Metrohm Autolab PGSTAT100, using NOVA 2.1 electrochemistry software interface. Cyclic voltammograms were recorded between –2.0 and + 1.8 V and scan rate of 100 mV $s^{-1}$. Differential pulse voltammograms were recorded from 0.0 to –2.0 V and 0.0 to + 1.8 V, with a step potential of 5 mV. All measurements were made using a three-electrode cell with a 3 mm glassy carbon working electrode (GCE), platinum wire counter electrode, and silver wire pseudo-reference electrode. Prior to each measurement, the GCE was polished using 0.05 μm alumina suspension on a micro-cloth polishing pad. Sample solutions were prepared using 1.0 mM analyte concentration, 0.1 M tetrabutylammonium hexafluorophosphate ($TBAPF_6$) supporting electrolyte in HPLC grade $CH_2Cl_2$, deoxygenated with Ar (g) before each voltammetric run. Reactivity of the complexes towards electrochemical $CO_2$ reduction was tested using the sample solutions as described above, purging the solutions with $CO_2$ for 30 min before starting analysis. All potentials from the cyclic voltammograms (CVs) and differential pulse voltammograms (DPVs) are reported relative to the silver wire pseudo-reference electrode, as addition of internal electrochemical standards (i.e. the $FcH^{0/+1}$ or $[Fe(\eta\text{-}C_5Me_5)_2]^{0/+1}$ couples respectively) to the analyte solutions caused significant shifts in the analyte's peak potentials, leading to the formation of additional secondary chemical reaction peaks, as well as the notable irreversibility of the internal standards' redox peaks between first and second scans. Additional results for complexes **1**–**4** are provided in SI section S3 and S4. CV was used initially to ascertain the redox behaviour of the studied complexes, while DPV, being a sensitive technique, was employed to get the exact peak potentials in the experiments performed.

### 2.4. Theoretical calculations

Structural optimisations and frequency calculations were performed on both the free ligands and all of the above reported complexes using Gaussian 16B.01 [38] at the Centre for High Performance Computing (CHPC) on the Lengau Supercomputer. The series of charged oxidation states that were modelled for each complex are labelled using "(n = integer)", where *n* represents the number of electrons that have been removed or added to the molecule (ex. "n = –1" representing the first oxidised state, and "n = +2" the second reduction state). A hybrid functional B3LYP [39,40] was employed with the def2SVP [41] split valence basis set on all atoms, including unrestricted basis functions for all calculations of open shell charged state molecules. Long range electron correlations resulting from electron delocalisation were accounted for with the addition of Grimme's D3 Empirical Dispersion function [42,43]. The effects of solvation were modelled using continuum potential surfaces functions [44,45] (denoted cPCM) for dichloromethane. The thermodynamic energies, frontier orbitals and electrostatic potential surfaces were calculated for all molecules and their charged states. Spin density plots were generated for charged state calculations to visualise the (de)localisation of the unpaired electrons.

A rigorous, systematic workflow was followed for the modelling of all complexes, ligands, and their associated oxidations states. The initial molecular geometries were derived from previously reported four and five coordinate aryl-BIAN transition metal complexes [9,11,15,22,46–52], and minimised using MM2 molecular mechanics with a minimum RMS gradient of 0.010. The gas phase geometries were further optimised using Gaussian 16B.01 [38], and optimisation confirmed to be at a minimum if a subsequent frequency calculation showed no imaginary vibrational frequencies. The optimised gas phase geometry of the (n = 0) state for each molecule was used as the initial guess for modelling the solvated molecular geometries in dichloromethane using cPCM. Similarly, the obtained solvated geometries were established to be at a minimum by confirming that there were no imaginary vibrational frequencies in the subsequent frequency calculations. FMO energy and visualisations calculated for complexes **1**–**4** are provided in SI section S5; and the total energies for all stationary points are available in SI section S6.

## 3. Results and discussion

### 3.1. Synthesis and characterisation

The initial rhodium(I) and iridium(I) 1,5-cyclooctadiene (cod) complexes of DippBIAN (**1a**, **1c**) and MesBIAN (**1b**, **1d**) were synthesised routinely through a standard ligand addition and anion substitution reaction starting from the free ligands, $KPF_6$, and the respective metals' cod-chloride dimer in a $CH_2Cl_2$ solution (Scheme 1) [21–23]. The dicarbonyl complexes **2a**–**d** were prepared from **1** by reaction with CO (g) and precipitation of the desired product with hexanes. The triethylphosphine ($PEt_3$) derivatives (**3a**, **b**) were synthesised from purified **2a** and **2b**. Iridium analogues of **3** were found to decompose during reaction work-up and over time, both in solution and in the solid state. The 5-coordinate cod-chloride derivatives (**4a**–**d**) were prepared in a procedure similar to that required for **1**, by simply excluding the $KPF_6$ salt from the reaction mixture [22]. Purification of **4** proved challenging due to their partial solubility in hexane. The lack of $PF_6^-$ counter ions in **4** was confirmed by the absence of any signals in the $^{19}F$ and $^{31}P$ NMR spectra.

Complexes **1**–**4** were characterised by NMR and FTIR spectroscopy, as well as high resolution mass spectrometry (see SI section S1). In the $^1H$ NMR spectra of the symmetric substituted free BIAN ligands, as well as the complexes **1** and **2**, the characteristic "*d-dd-d*" acenaphthalene

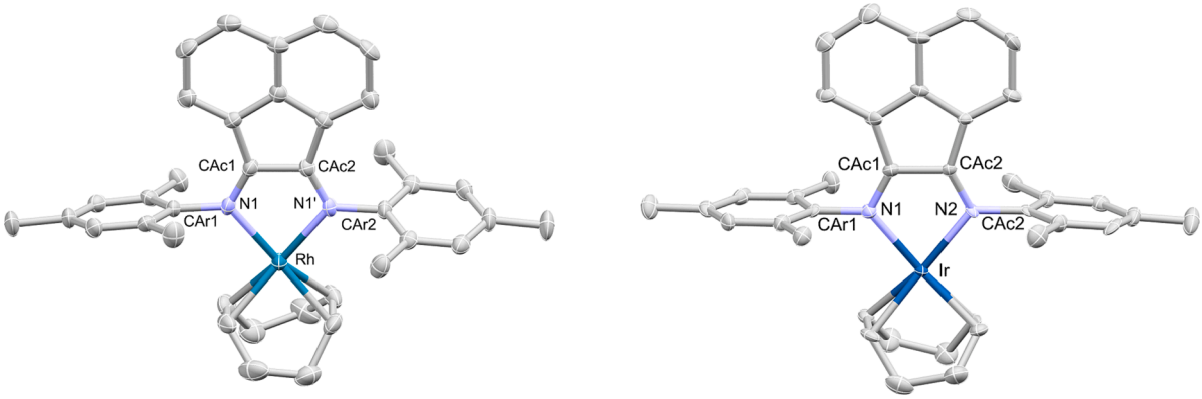


**Fig. 1.** Crystal structure of **1b** (left) and **1d** (right) as determined by single crystal XRD, thermal ellipsoids are presented at 50% probability. Hydrogens, solvent molecules and anions have been omitted for clarity.

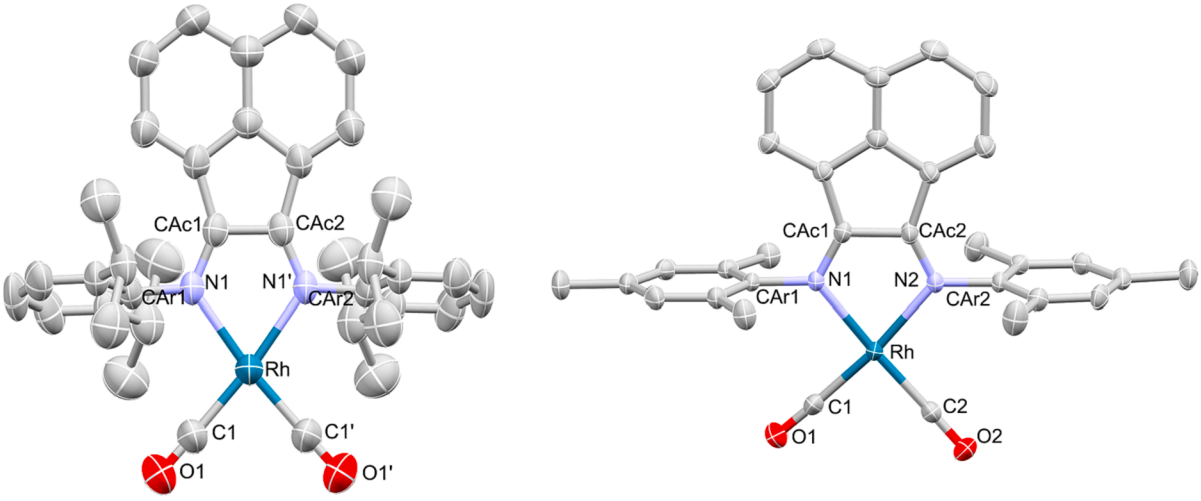


**Fig. 2.** Crystal structure of **2a** (left) and **2b** (right) as determined by single crystal XRD, thermal ellipsoids are presented at 50% probability. Hydrogens, solvent molecules and anions have been omitted for clarity.

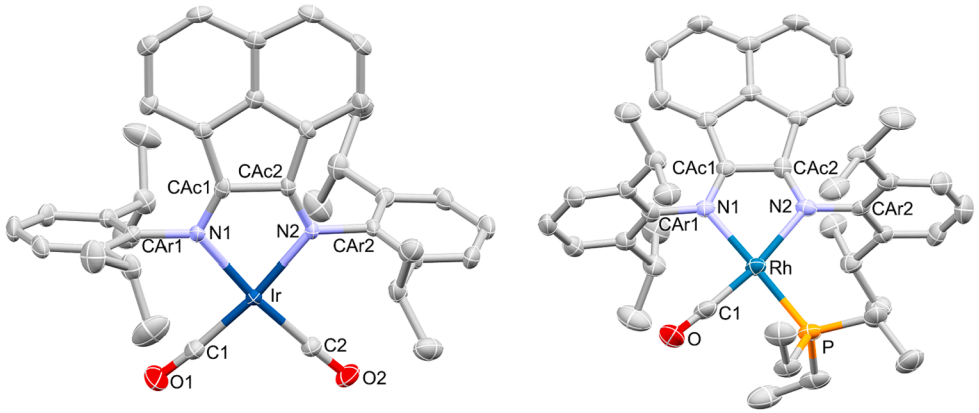


**Fig. 3.** Crystal structure of **2c** (left) and **3a** (right) as determined by single crystal XRD, thermal ellipsoids are presented at 50% probability. Hydrogens, solvent molecules and anions have been omitted for clarity.

splitting pattern is observed. The absence of this splitting pattern in the proton spectra of **3a**, **3b** and **4a** indicates a loss of symmetry in the coordination sphere. Instead, the inequivalent electronic environment of the six acenaphthalene protons result in the formation of multiple doublet signals between 7.7 and 7.2 ppm, overlapping with the phenyl-aromatic protons signals. The Dipp-substituent isopropyl-CH's of **3a** and **4a** appear as two septets corresponding to the isopropyl which is nearest to (downfield shifted) or furthest away from (upfield shifted) the sterically encumbered Cl and $PEt_3$ ancillary ligands. Conversely, the $^{1}H$ and $^{13}C$ spectra for **4b**–**d** exhibit a more symmetrical molecular geometry in solution compared to the distorted square pyramidal structure which has been reported for **4a** [22]. The coordinated cod-alkenes of complexes **4b**–**d** display a single olefinic signal between 4.0 and 3.7 ppm, whereas two olefinic singlets are observed for complex **4a** at 4.23 and 3.85 ppm. The higher field chemical shifts observed for the cod-chloride complexes **4b**–**d** clearly distinguish them from their cationic analogues (**1b**–**d**), whilst confirmation of the molecular structure is obtained from the crystal structure of **4d** (*vide infra*).

As expected, the carbonyl carbon resonance for the dicarbonyl complexes **2a**, **2b** and **2d** are observed at 180.2, 180.19 and 180.4 ppm respectively in the $^{13}C$ NMR spectra, whereas the carbonyl carbon resonance for the carbonyl-phosphine complexes **3a** and **3b** appear more upfield at 177.3 and 177.6 ppm respectively. In the FTIR spectra of complexes **2**, two carbonyl vibrational bands were observed between 2100 and 2000 $cm^{-1}$, whereas singular carbonyl stretching frequencies were observed for complexes **3a** and **3b** at 1991 and 1989 $cm^{-1}$ respectively.

### 3.2. Crystallography

Single crystals of complexes **1b**, **1d**, **2a**, **2b**, **2c**, **3a** and **4c** suitable for XRD analysis were prepared through slow evaporation of $CH_2Cl_2$ or $CDCl_3$ solutions, and the molecular structures are shown in Figs. 1–4 (and Figures S58–S64). A selection of bond lengths, angles and dihedral angles are presented in Table 1 below, and Tables S1–S3.

The centre of each cod-alkene bond was utilised as a measurement point for the calculation of geometric parameters. The coordination geometries about the 4-coordinate metal centres of complexes **1**–**3** are described in terms of the geometric parameter "$\tau_4$", defined by Yang *et al.* [53], where the values of $\tau_4 = 0.00$ represents a square planar coordination, and $\tau_4 = 1.00$ a tetrahedral coordination geometry. The 5-coordinate geometry of complex **4c** is described in terms of the geometric parameter $\tau_5$ defined by Addison *et al.* [54], where $\tau_5 = 0.00$ represents a square pyramidal coordination, and $\tau_5 = 1.00$ a trigonal bipyramidal coordination geometry about the metal. The coordination spheres of complexes **1**–**3** can be described as slightly distorted square planar, as expected for Rh(I) and Ir(I) complexes, with $\tau_4 = 0.06$–$0.10$.

The bisimine moieties in all of the complexes were largely co-planar, with the N1=$C_{Ac1}$–$C_{Ac2}$=N2 torsion angles for **1b**, **1d** (Fig. 1) and **2c** (Fig. 3, left) showing only slight distortion (–3.0(8)°, 2.6(12)° and 2.7

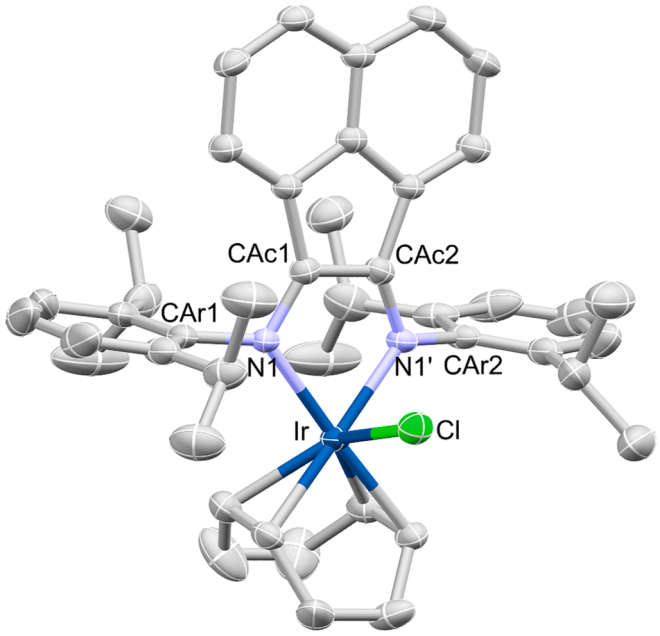


**Fig. 4.** Crystal structure of **4c** as determined by single crystal XRD, thermal ellipsoids are presented at 50% probability. Hydrogens, solvent molecules and anions have been omitted for clarity.

(6)° respectively). The average N1–M–N2 bite angle enforced by coordination to the rigid bisimine ligand is 78.6°, except for **2a** where the small bite angle (N1–Rh–N1′ 69.4(2)°) is enforced by coordination to the rigid bisimine ligand as well as the small angle between the two carbonyl ligands (C1–Rh–C1′ 80.8(4)° (Fig. 2, left)) resulting in an almost rectangular geometry of the coordination centre. Steric constraints imposed on the bulky Dipp-substituents by crystal packing effects in the present structure contribute to the angular rotation of the Dipp-substituents relative to the acenaphthalene plane (*ca.* 13.3°) and the distortions observed in the aryl-aryl, and alkyl-alkyl C-C bond lengths of the ligand. All complexes except **2a** and **4c** showed a $C_{Ac}$–N–$C_{Ar}$ bond angle of *ca.* 119°, consistent with a $sp^2$-hybridized nitrogen (Table S2).

The asymmetric coordination structure of **3a** (Fig. 3, right) results in differences in the Rh–N bond lengths (Rh–N1 2.3053(13) and Rh–N2 2.163(4) Å) caused by the stronger *trans*-influence of the phosphine compared to the carbonyl ligand. The Rh–N1 bond *trans* to the triethylphosphine ligand is roughly 0.2 Å longer than is observed in any of the other Rh(I) complexes (av. 2.11 Å), while the.

Rh–N2 bond *trans* to the carbonyl ligand is comparable to the analogous bond length observed in **2a** (2.135(4) Å).

The five-coordinate cod-chloride, **4c** (Fig. 4), has a square pyramidal geometry ($\tau_5 = 0.00$) with slight angular distortion of the axial chlorido ligand as it is positioned nearly perpendicular to the bisimine nitrogens (avg. 88.3(6)°), but bent away from the steric bulk of the cod ligand and slightly towards the main acenaphthalene plane (79.66°). This is partly achieved by the five-membered metallocycle, formed between the bisimine moiety and iridium, deforming to a greater extent than is observed in any of the other complexes and adopting an "envelope" geometry more reminiscent of a cyclopropane ring. The Ir–Cl bond length is (2.4754(11) Å) is in the upper limit of the average reported bond lengths for Ir(I) or Ir(III) complexes [55–62], similar to the elongated Rh–Cl bond observed for the rhodium(I) analogue [22].

The relationship between the N=$C_{Ac}$ and $C_{Ac}$–$C_{Ac}$ bond lengths in the bisimine moiety of BIAN ligand has often been applied as an indicator of the oxidation state of the coordinated ligand [1,16,18,63–65]. The average N=$C_{Ac}$ and $C_{Ac}$–$C_{Ac}$ bond lengths observed in the crystal structures of five of **1b**, **1d**, **2b**, **2c** and **3a** (av. 1.28 Å and 1.50 Å respectively) are indicative of a nitrogen–carbon double bond and carbon–carbon single bond characteristic of neutral BIAN ligands. The elongated N=$C_{Ac}$ (1.350(6) Å) and shortened $C_{Ac}$–$C_{Ac}$ (1.381(9) Å) bond lengths in **2a** correspond to values previously reported for a dianionic [DippBIAN$^{2-}$] quinonate ligand [1,16,63,64,66,67]; whereas the N=$C_{Ac}$ (1.321(4) Å) and.

$C_{Ac}$–$C_{Ac}$ (1.447(6) Å) bond lengths of **4c** agree more closely with previous reports of a radical monoanionic [DippBIAN$^{1-}$] semiquinonate ligand [1,16,18,63–65]. In the crystal structure of **2a**, however, the rhodium centre adopts a square planar geometry which is indicative of a Rh(I) complex (as opposed to an octahedral Rh(III) centre), and the absence of additional counter cations further negate the possibility of a

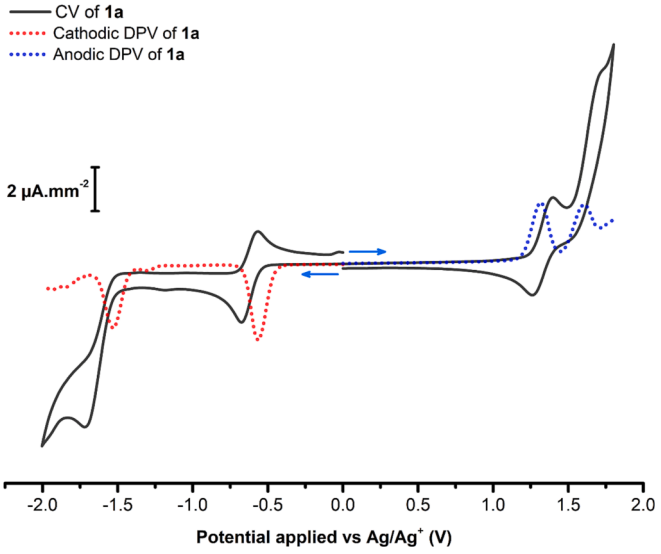


**Fig. 5.** CV and DPV of **1a** [RhDB(cod)]$PF_6$ recorded in $CH_2Cl_2$ with 1.0 mM analyte and 0.1 M $TBAPF_6$ supporting electrolyte.

**Table 1**
Selected bond lengths (Å), bond angles (°) and dihedral angles (°) from XRD data. M = Metal; Ac = Acenaphthalene imine carbon; L = ancillary ligand. † Half of molecule is present in asymmetric unit, therefore selected bond lengths and angles are duplicated in the complex structure. ‡ Imine-N *trans* to $PEt_3$.

| | **1b** | **1d** | **2a** | **2b** | **2c** | **3a** | **4c** |
|---|---|---|---|---|---|---|---|
| **M–N** | 2.100(4)† | 2.100(7)2.097 (7) | 2.135(4)† | 2.0728(17)2.0898 (16) | 2.082(3)2.083 (3) | 2.3053(13)‡2.163 (4) | 2.096(2)† |
| **N–$C_{Ac}$** | 1.276(7)† | 1.291(11)1.280 (11) | 1.350(6)† | 1.285(3)1.289 (2) | 1.279(5)1.277 (5) | 1.278(6)1.289 (6) | 1.321(4)† |
| **$C_{Ac1}$–$C_{Ac2}$** | 1.492(10) | 1.495(13) | 1.381(9) | 1.501(3) | 1.500(5) | 1.495(6) | 1.447(6) |
| **M–L** (L = CO, $PEt_3$, Cl) | | | 1.897(6)† | 1.871(2)1.875 (2) | 1.873(5)1.861 (4) | Rh–P 2.3053(13)Rh–CO 1.814 (6) | Ir–Cl 2.4754(11) |
| **$N_1$–M–$N_2$** | 78.9(2) | 78.8(3) | 69.4(2) | 79.78(6) | 78.47(13) | 77.30(15) | 78.49(13) |
| **L–M–L** (L = CO, $PEt_3$) | | | 80.8(4) | 89.89(8) | 91.69(19) | 85.24(16) | |
| **N–$C_{Ac1}$–$C_{Ac2}$–N** | –3.0(8) | 2.6(12) | 0.0(6) | 0.4(3) | 2.7(6) | 0.2(7) | 0.0(4) |

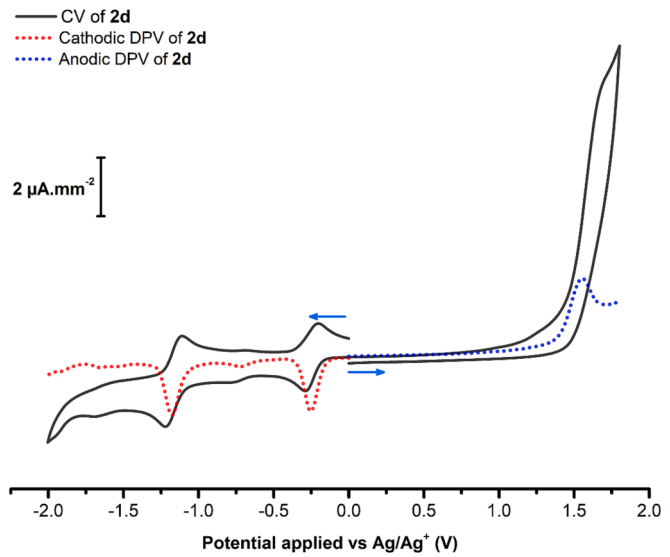


**Fig. 6.** CV and DPV of **2d** [IrMB(CO)$_2$]PF$_6$ recorded in $CH_2Cl_2$ with 1.0 mM analyte and 0.1 M TBAPF$_6$ supporting electrolyte.

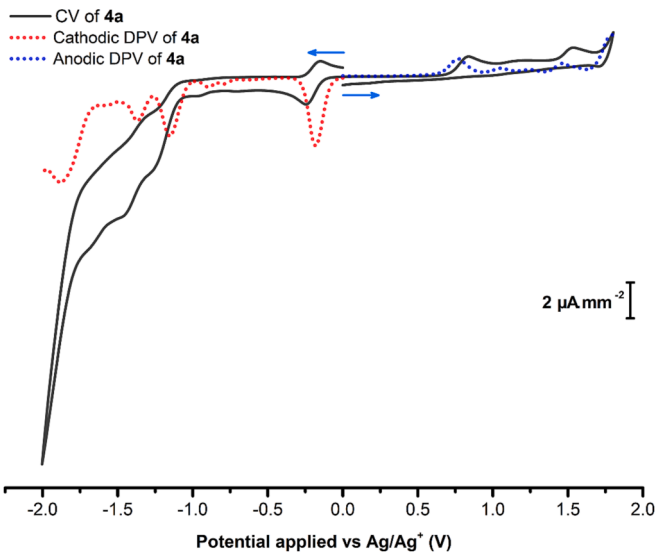


**Fig. 8.** CV and DPV of **4a** [RhDB(cod)Cl] recorded in $CH_2Cl_2$ with 1.0 mM analyte and 0.1 M TBAPF$_6$ supporting electrolyte.

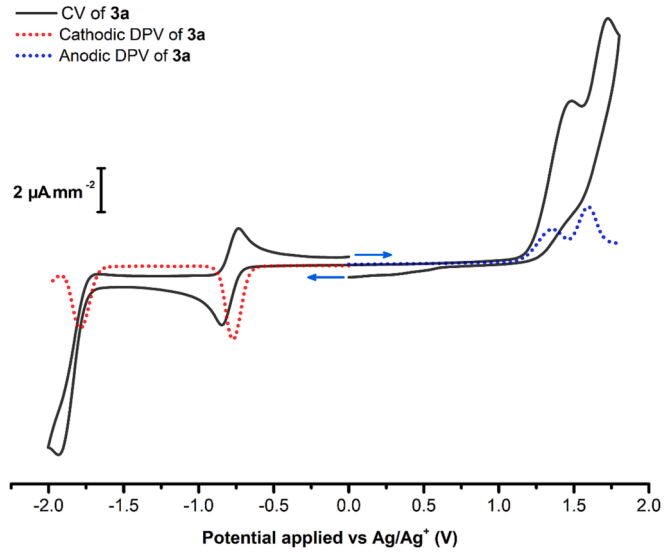


**Fig. 7.** CV and DPV of **3a** [RhDB(CO)(PEt$_3$)]PF$_6$ recorded in $CH_2Cl_2$ with 1.0 mM analyte and 0.1 M TBAPF$_6$ supporting electrolyte.

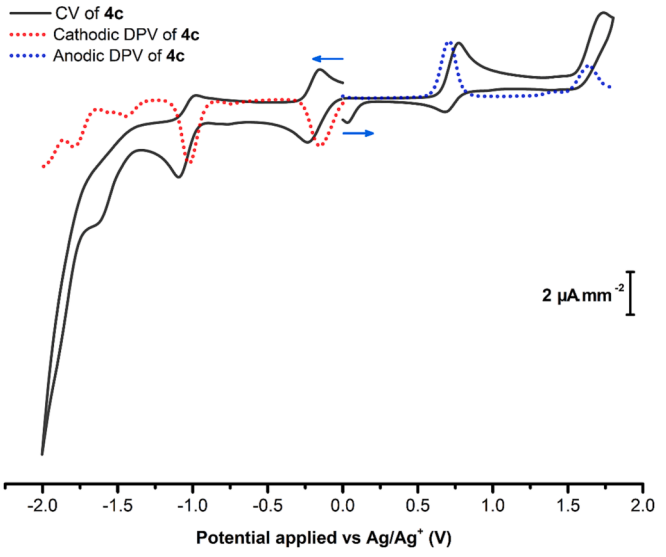


**Fig. 9.** CV and DPV of **4c** [IrDB(cod)Cl] recorded in $CH_2Cl_2$ with 1.0 mM analyte and 0.1 M TBAPF$_6$ supporting electrolyte.

reduced ligand coordinated in **2a**. Similarly, in the structure of **4c** the neutral iridium centre adopts a square pyramidal geometry similar to that observed for previously reported structure of **4a** [22], with rhodium in oxidation state +1, making the coordination of a reduced ligand unlikely. No additional evidence was obtained from the characterisation data, computational modelling or electrochemical analyses to substantiate the assignment of anionic charge to the DippBIAN ligands in **2a** and **4c**.

### 3.3. Electrochemical behaviour and molecular orbital calculations

In the electrochemical studies, all compounds showed an electrochemically reversible first reduction event at potentials less negative than –1.0 V (vs Ag/Ag$^+$) (see Figs. 5–9). Reduction events of the Rh complexes are observed at more negative potentials than the iridium complexes, except with complexes **4a** and **4b**. All oxidation events were irreversible except the first oxidation of **1a**, **1c**, **2b** and **4c**, as well as the second oxidation of **4d**. Inspection of the FMO distributions for these complexes indicate that the first and second reduction events in all cases are ligand centred and delocalised across the bisimine N=C–C=N moiety, whereas the first oxidation event in all cases is metal centred, with the second and third oxidations delocalised across one of the aryl-substituents each. These observations are in good correlation to electrochemical, EPR and computational results of previously reported BIAN complexes of various transition metals [22,68–74]. The redox behaviour of complexes **1a**, **2d**, **3a**, **4a** and **4c** are discussed here as representative examples for comparative purposes. The electrochemistry data and calculated molecular orbitals for all compounds are available in the SI sections S3 and S5, respectively.

Cathodic scans of complex **1a** displayed a reversible reduction at –0.56 V, and an irreversible reduction at –1.53 V (Fig. 5). A reversible oxidation is observed at +1.31 V, along with a subsequent irreversible oxidation at +1.61 V. Inspection of the LUMO of **1a** indicates that the first reduction is mainly delocalised across the acenaphthalene rings and bisimine moiety (Figure S85), with minor contributions visible from the cod-alkene orbitals, while the second reduction appears chiefly localised

**Table 2**
Selected bond lengths (Å) from cPCM DFT data for **4a** and **4c** modelled in different oxidation states.

| Complex | Rh–Cl Bond length | Complex | Ir–Cl Bond length |
|---|---|---|---|
| **4a**$^{+}$ [RhDB(cod)Cl]$^{+}$ (n = –1) | 2.5120 | **4c**$^{+}$ [IrDB(cod)Cl]$^{+}$ (n = –1) | 2.4110 |
| **4a** [RhDB(cod)Cl] (n = 0) | 2.6130 (2.5908(12))[a] | **4c** [IrDB(cod)Cl] (n = 0) | 2.4269 (2.4754(11))[b] |
| **4a**$^{-}$ [RhDB(cod)Cl]$^{-}$ (n = +1) | 4.6886 | **4c**$^{-}$ [IrDB(cod)Cl]$^{-}$ (n = +1) | 2.4478 |
| **4a**$^{-2}$ [RhDB(cod)Cl]$^{-2}$ (n = +2) | 5.0332 | **4c**$^{-2}$ [IrDB(cod)Cl]$^{-2}$ (n = +2) | 2.4637 |
| **4a**$^{-3}$ [RhDB(cod)Cl]$^{-3}$ (n = +3) | 5.5416 | **4c**$^{-3}$ [IrDB(cod)Cl]$^{-3}$ (n = +3) | 2.5896 |

[a]Experimentally measured Rh − Cl bond length from SC-XRD data previously reported [22]. [b]Experimentally measured Ir − Cl bond length from SC-XRD data (see Table 1).

in a π*-antibonding MO comprised of contributions from the acenaphthalene ring and bisimine moiety. These FMOs are indicative of ligand-centred reductions taking place, illustrating the BIAN ligand's ability to stabilise additional electron density across its aromatic moieties while coordinated.

Cathodic scans of the dicarbonyl complexes **2a**, **2c** and **2d** present a pair of reversible reductions between –0.20 and –1.55 V, while **2b** showed one reversible reduction and one irreversible reduction (Fig. 6, and Figures S70–S72). The cathodic scans of **3a** under Ar (Fig. 7) appear similar to those of **1a**, with a reversible reduction at –0.77 V and an irreversible reduction at –1.79 V, shifted to more negative potentials by roughly 0.2 V due to the increased electron donating ability of the phosphine ligand. When examining the anodic scan of **3a**, oxidations are observed at +1.36 V and +1.60 V, similar to those observed for **1a**.

The spatial distribution of the FMOs across the acenaphthalene and bisimine N=C–C=N moieties for the first and second (Figures S99 and S101) reduced states of **2d** and **3a** closely resemble those of **1a**, indicating that these reductions are ligand-centred events. The (n = +1) α-LUMOs of **2d** and **3a** include additional antibonding symmetry contributions between the carbon and oxygen of the carbonyl ligands, whereas the cod-ligand in **1a** and the phosphine in **3a** showed little contribution to these MOs. The symmetry of these α-LUMO orbital interactions indicate a partial increase in the π-backbonding from the metal to the carbonyl ligands during the first reduction event.

Complex **4a** presented a reversible reduction event at –0.18 V (Fig. 8), as well as irreversible second and third reductions at –1.15 V and –1.37 V with an upsurge in cathodic current at potentials more negative than –1.5 V. Two irreversible oxidation peaks are identified at +0.77 V and +1.46 V. The reduction peaks are shifted to less negative potentials with respect to **1a** due to the presence of the electron donating chlorido ligand in **4a**, whereas the oxidation peaks are shifted to more positive potentials.

The redox profile of **4c** (Fig. 9) reveals three reduction events at –0.16 V, –1.02 V and –1.45 V, with an upsurge in cathodic current at potentials more negative than –1.7 V. The first two reductions of **4c** and **4d** are reversible (Figure S75) and shifted to more positive potentials compared to those of **4a**. In addition, only the first reduction events of **4a** and **4b** were reversible (Figure S74), indicating that the iridium analogues of the cod-Cl complexes are able to stabilise a higher negative charge on the complex than their rhodium counterparts. Two oxidation events were identified for complex **4c** at +0.71 V and +1.64 V, comparable to the oxidation potentials of **4a**, however, the first oxidation of **4c** presents as a quasi-reversible event.

Similar to the MO descriptions of **1a** and **3a**, the first reduction of **4a** and **4c** is delocalised between the bisimine moiety and acenaphthalene rings, with minor contributions from the chloride and alkene co-ligands visible (Figures S105 and S109). The second reduction event is likewise confined to the bisimine and acenaphthalene orbitals. Unlike the previously discussed complexes, the charge localisation for the (n = +3) state of complexes **4a**–**d** (Figures S105–S111) is not immediately apparent since the orbital distributions associated with the (n = +3) HOMO and (n = +2) LUMO are markedly different.

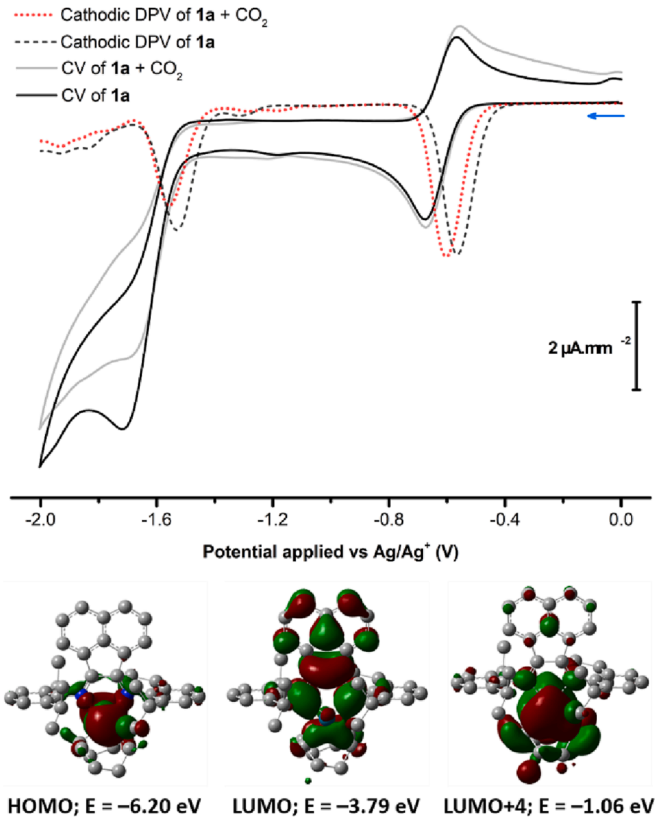


**Fig. 10.** CV and DPV of **1a** [RhDB(cod)]$PF_6$ in the presence of $CO_2$ or Ar, recorded in $CH_2Cl_2$ with 1.0 mM analyte and 0.1 M $TBAPF_6$ supporting electrolyte. The HOMO, LUMO and LUMO +4 orbital spatial orientations are presented below with their associated energies, calculated at B3LYP-D3/def2-SVP level of theory in $CH_2Cl_2$ using cPCM.

The reduction events of **1c** and **1d** (Figures S68–S69) have a similar appearance to those of the cod-Cl complexes **4a**–**d** (Figs. 8–9, Figures S74–S75), with a steep upsurge in reduction current after the third reduction event (avg. < –1.5 V) akin to the current increase that is observed in the CVs of the free ligands (Figures S65–S66). DFT calculations showed an elongation of the M−Cl bond with each reduction step (Table 2). However, the calculated bond distance of Rh–Cl in **4a**$^{-}$, **4a**$^{-2}$ and **4a**$^{-3}$ are significantly more elongated than the corresponding Ir–Cl bonds in the analogous complexes **4c**$^{-}$, **4c**$^{-2}$ and **4c**$^{-3}$, pointing to the absence of a bonding interaction between the metal center and chlorido ligand in the reduced complexes **4a**$^{-}$–**4a**$^{-3}$. This is in accord with results previously reported for the octahedral *mer*-[RhDB(Cl)$_3$($H_2O$)], suggesting the steep current increase may be due to the irreversible reductive dissociation of the chlorido ligand from the complexes, with subsequent/concurrent dissociation of the BIAN ligand as decomposition of the complexes take place [23]. Furthermore, it is worth noting here that the studies did not use scan rate variations as most of the redox events for the reported compounds are irreversible.

### 3.4. Electrochemical $CO_2$ reduction and interactions

Reactivity of the complexes towards electrochemical $CO_2$ reduction was tested using the sample solutions as described above, purging the solutions with technical grade $CO_2$ for 30 min before running the voltammograms (see Figs. 10–14). Complex **2d** showed a modest increase in cathodic current (10 μA) at potentials more negative than –1.6 V

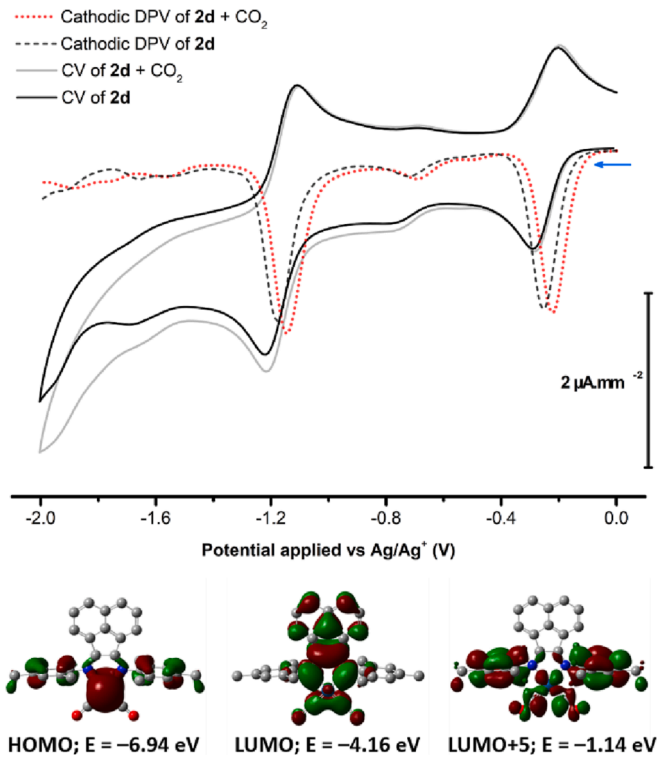


**Fig. 11.** CV and DPV of **2d** $[IrMB(CO)_2]PF_6$ in the presence of $CO_2$ or Ar, recorded in $CH_2Cl_2$ with 1.0 mM analyte and 0.1 M $TBAPF_6$ supporting electrolyte. The HOMO, LUMO and LUMO +5 orbital spatial orientations are presented below with their associated energies, calculated at B3LYP-D3/def2-SVP level of theory in $CH_2Cl_2$ using cPCM.

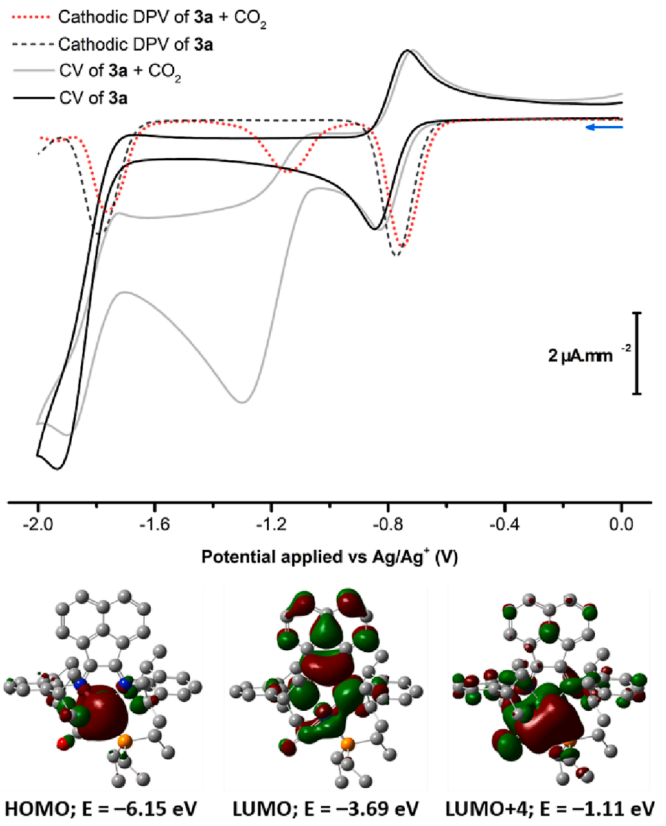


**Fig. 12.** CV and DPV of **3a** $[RhDB(CO)(PEt_3)]PF_6$ in the presence of $CO_2$ or Ar, recorded in $CH_2Cl_2$ with 1.0 mM analyte and 0.1 M $TBAPF_6$ supporting electrolyte. The HOMO, LUMO and LUMO +4 orbital spatial orientations are presented below with their associated energies, calculated at B3LYP-D3/def2-SVP level of theory in $CH_2Cl_2$ using cPCM.

(Fig. 11), as well as a 30–55 mV positive shift in reduction and oxidation potentials, indicating interaction between the complex and $CO_2$ in solution. An additional irreversible reduction peak was observed at –1.14 V in the cathodic scans of **3a** in the presence of $CO_2$ (Fig. 12), along with *ca.* 20 mV positive shift of all reduction and oxidation peak potentials. The increase in cathodic current (5 $\mu A.mm^{-2}$) was only observed between –1.3 and –1.6 V, suggesting that the [**3a**$^-$] anion intermediate generated during the first reduction at –0.77 V forms an adduct with $CO_2$, which further reacts with $CO_2$ to drive the reaction forward [19,23,28,75–81]. Additional electrochemical $CO_2$ reactivity data for the reported compounds are presented in the SI sections S4.

The reduction profiles of **1a** (Fig. 10), **4a** (Fig. 13), and **4c** (Fig. 14) appear largely unaffected by the presence of $CO_2$ in the solution, however, a +2.5 $\mu A.mm^{-2}$ decrease in cathodic current is observed beyond –1.3 V along with the disappearance of the DPV peak for **4a** at –1.88 V.

It has been well-established via Walsh diagrams that transferring electron density to the LUMO of $CO_2$ enables the molecule to bend, thereby favouring its reduction [82]. The shift of the 1st reduction and 1st oxidation waves indicated in Figs. 10–14 (as well as Table 3) are in line with literature reports of $CO_2$ reduction [19,23,28,76,77,79,80,83], leading us to conclude an interaction of $CO_2$ with the reported complexes. An increase in cathodic current is observed in the case of complex **2d**, however, we did not observe similar $CO_2$ reduction activity as previously reported for **4a** [22,23]. However, this can be attributed to the following reasons: 1) $CO_2$ is less soluble in $CH_2Cl_2$ than in $CH_3CN$ or dimethyl formamide (DMF); 2) the reported complexes were not stable in DMF or $CH_3CN$, limiting our experiments to a non-coordinating $CH_2Cl_2$ solvent; 3) the absence of a sacrificial proton source in the electrolyte medium also precludes a number of possible $CO_2$ reduction mechanisms, and will be included in future investigations [23,28,76–78]. In addition, the cathodic behaviour observed for our complexes correlate well with a recent report on Ag(I)$BIAN_2$ complexes as efficient electrocatalysts for $CO_2$ electroreduction [81].

In order to understand why complex **3a** displayed better $CO_2$ electroreduction reactivity, we looked at the spatial orientations of the HOMO, LUMO and higher order LUMOs of the above studied complexes described *vide supra*, Figs. 5, 10–13 and S74–S84. The higher order LUMOs indicated a near-HOMO character for the complex **3a** at LUMO +4. However, for the other complexes discussed in this article, the near-HOMO character is found beyond LUMO +3 thus leading to potential drops ($\Delta E_{(LUMO)}$) as indicated in Table 3. The complex **3a** shows a lowest potential drop of 2.58 eV which could facilitate the movement of electrons from donor to acceptor thereby advancing the $CO_2$ reduction [84,85]. This observation also compliments our crystallographic data which revealed a stronger *trans*-influence of the $PEt_3$ group in **3a** leading to asymmetric differences at the coordination site.

## 4. Conclusion

A series of rhodium(I) and iridium(I) complexes of Dipp- and Mes-BIAN are reported, featuring either square planar or square pyramidal coordination geometries. The square planar crystal structures of **1b** $[RhMB(cod)]PF_6$, **1d** $[IrMB(cod)]PF_6$, **2a** $[RhDB(CO)_2]PF_6$, **2b** $[RhMB(CO)_2]PF_6$, **2c** $[IrDB(CO)_2]PF_6$ and **3a** $[RhDB(CO)(PEt_3)]PF_6$ are reported, as well as the square pyramidal **4c** [IrDB(cod)Cl] structure. The bisimine moiety bond lengths within the structures of **2a** and **4c** deviate from those expected for a neutral BIAN ligand, and suggest that the DippBIAN ligand in these complexes is in a reduced state. However, no additional evidence from multi-technique analyses were observed which would support assigning the ligands a negative charged state. This anomalous data is indicative of non-innocent behaviour of the DippBIAN ligand within **2a** and **4c** – accepting additional electron density from the

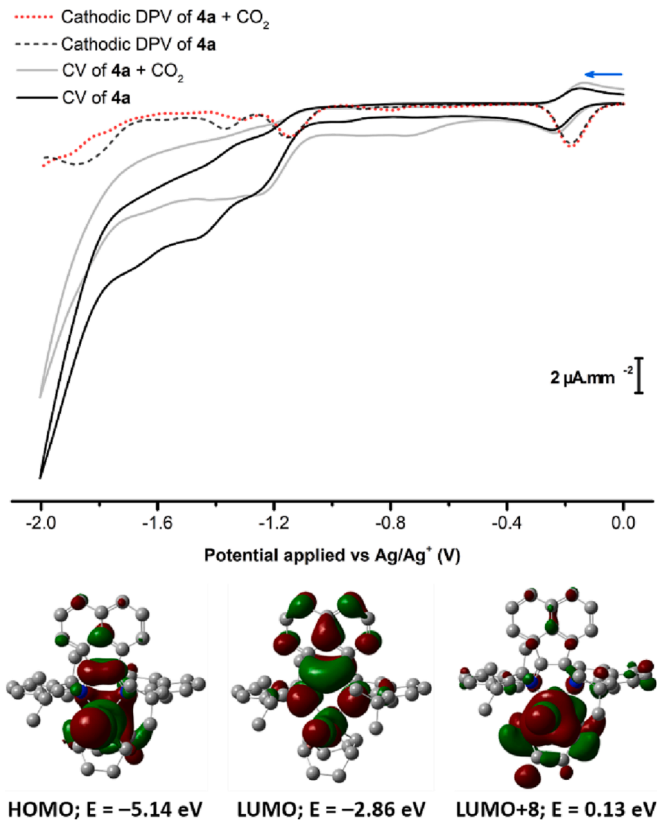


**Fig. 13.** CV and DPV of **4a** [RhDB(cod)Cl] in the presence of $CO_2$ or Ar, recorded in $CH_2Cl_2$ with 1.0 mM analyte and 0.1 M $TBAPF_6$ supporting electrolyte. The HOMO, LUMO and LUMO +8 orbital spatial orientations are presented below with their associated energies, calculated at B3LYP-D3/def2-SVP level of theory in $CH_2Cl_2$ using cPCM.

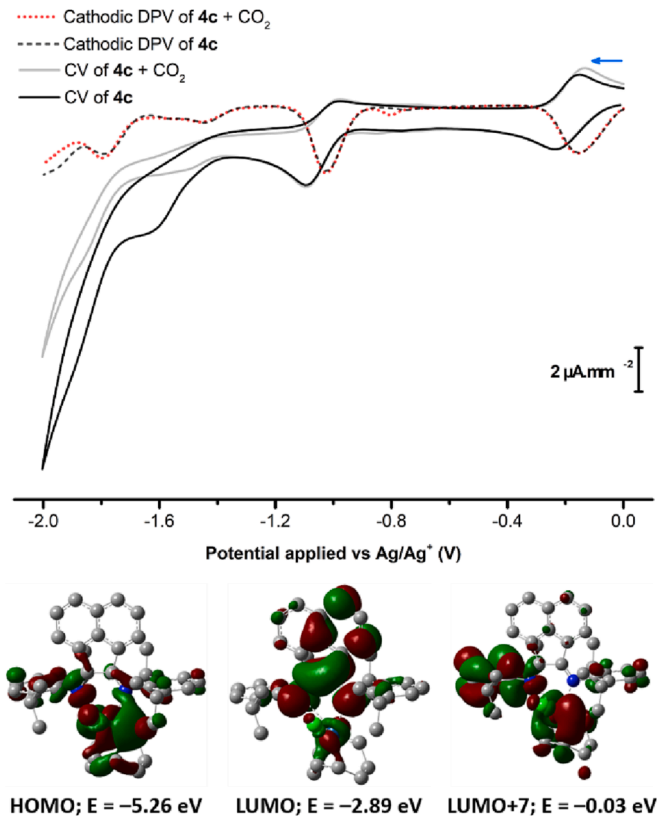


**Fig. 14.** CV and DPV of **4c** [IrDB(cod)Cl] in the presence of $CO_2$ or Ar, recorded in $CH_2Cl_2$ with 1.0 mM analyte and 0.1 M $TBAPF_6$ supporting electrolyte. The HOMO, LUMO and LUMO +7 orbital spatial orientations are presented below with their associated energies, calculated at B3LYP-D3/def2-SVP level of theory in $CH_2Cl_2$ using cPCM.

metal centre due to push–pull mechanism between the ancillary ligands and BIAN.

The systematic electrochemical study in non-coordinating solvent $CH_2Cl_2$, revealed that all the complexes feature at least one reversible, ligand-centred, reduction event at potentials less negative than –1.0 V; well above the reduction potential of the free ligands. Complex **1a** [RhDB(cod)]$PF_6$ is the only complex to show a fully reversible oxidation, while **1b**, **2b**, **4c** and **4d** [IrMB(cod)Cl] display oxidation events which are electrochemically reversible, but not chemically reversible on the timescale of the scan rate employed.

Complex **2d** [$IrMB(CO)_2$]$PF_6$ shows a positive shift in reduction potentials and a modest increase in reduction current between –1.0 and –1.9 V upon addition of $CO_2$ to the electrochemical cell solutions, while **3a** [RhDB(CO)($PEt_3$)]$PF_6$ exhibits the formation of an additional reduction peak at –1.14 V (with concomitant increase in anodic current). These changes indicate an associative interaction between the complexes and $CO_2$ which are well corroborated with our theoretical calculations and analysis on the higher order LUMOs and crystallographic structure analysis. The results in this study lay a strong foundation for this class of compounds to be used in renewable energy research, especially into $CO_2$ electroreduction studies.

## Declaration of Competing Interest

The authors declare that they have no known competing financial interests or personal relationships that could have appeared to influence the work reported in this paper.

**Table 3**
A summary of the DPV peak potentials (in V vs $Ag/Ag^+$) recorded for complexes **1–4** in solutions saturated with either Ar (g) or $CO_2$ (g). Key: * Electrochemically reversible events. § New peak observed in the $CO_2$ saturated solutions. # $\Delta E_{(LUMO)} = E_{LUMO+x} - E_{LUMO}$ (in eV), where LUMO +x is the higher order LUMO with near-HOMO character as shown in Figs. 10–14.

| Compound | Red. 2 | Red. 1 | Ox. 1 | $\Delta E^{\#}_{(LUMO)}$ | LUMO +x |
|---|---|---|---|---|---|
| **1a** | –1.53 | –0.56* | +1.31* | 2.73 | LUMO +4 |
| **1a** + $CO_2$ | –1.56 | –0.60* | +1.40* | | |
| **2d** | –1.18* | –0.25* | +1.56 | 3.02 | LUMO +5 |
| **2d** + $CO_2$ | –1.14* | –0.22* | +1.61 | | |
| **3a** | –1.79 | –0.77* | +1.36 | 2.58 | LUMO +4 |
| **3a** + $CO_2$ | –1.14§ | –0.75* | +1.38 | | |
| **4a** | –1.15 | –0.18* | +0.77 | 2.99 | LUMO +8 |
| **4a** + $CO_2$ | –1.14 | –0.18* | +0.79 | | |
| **4c** | –1.02* | –0.16* | +0.70 | 2.86 | LUMO +7 |
| **4c** + $CO_2$ | –1.03* | –0.16* | +0.70 | | |

## Data availability

Data will be made available on request.

## Acknowledgements

The authors gratefully acknowledge the University of Pretoria, the National Research Foundation, South Africa (Renewable and Sustainable Energy Masters and Doctoral Scholarship), and Sasol Technology R&D Pty. Ltd. (South Africa) for financial support; the Centre for High Performance Computing (CHPC Cape Town, South Africa, http://www.chpc.ac.za) for access to utilise their computational resources; and Dr M.

Wooding for her assistance in conducting the mass spectrometry analyses. SGR thanks the South African National Research Foundation (NRF) for research support via the CSUR funding element, UID: 116317.

## Appendix A. Supplementary data

Supplementary data to this article can be found online at https://doi.org/10.1016/j.poly.2023.116350.

## References


[1] M. Viganò, F. Ferretti, A. Caselli, F. Ragaini, M. Rossi, P. Mussini, P. Macchi, Easy Entry into Reduced Ar-BIANH 2 Compounds: A New Class of Quinone/Hydroquinone-Type Redox-Active Couples with an Easily Tunable Potential, Chem. Eur. J. 20 (2014) 14451–14464, https://doi.org/10.1002/chem.201403594.

[2] K. Hasan, E. Zysman-Colman, Synthesis, UV-Vis and CV properties of a structurally related series of bis(Arylimino)acenaphthenes (Ar-BIANs), J. Phys. Org. Chem. 26 (2013) 274–279, https://doi.org/10.1002/poc.3081.

[3] R. van Asselt, C.J. Elsevier, Homogeneous catalytic hydrogenation of alkenes by zero-valent palladium complexes of cis-fixed dinitrogen ligands, J. Mol. Catal. 65 (1991) L13–L19. 10.1016/0304-5102(91)85057-9.

[4] R. van Asselt, C.J. Elsevier, W.J.J. Smeets, A.L. Spek, R. Benedix, Synthesis and characterization of rigid bidentate nitrogen ligands and some examples of coordination to divalent palladium. X-ray crystal structures of bis (p-tolylimino) acenaphthene and methylchloro [bis(o, o′-diisopropylphenyl-imino) acenaphthene] palla, Recl. Des Trav. Chim. Des Pays-Bas. 113 (1994) 88–98, https://doi.org/10.1002/recl.19941130204.

[5] L.K. Johnson, C.M. Killian, M. Brookhart, New Pd(II)- and Ni(II)-Based Catalysts for Polymerization of Ethylene and α-Olefins, J. Am. Chem. Soc. 117 (1995) 6414–6415, https://doi.org/10.1021/ja00128a054.

[6] V.C. Gibson, S.K. Spitzmesser, Advances in Non-Metallocene Olefin Polymerization Catalysis, Chem. Rev. 103 (2003) 283–316, https://doi.org/10.1021/cr980461r.

[7] P. Preishuber-Pflugl, M. Brookhart, Highly active supported nickel diimine catalysts for polymerization of ethylene, Macromolecules. 35 (2002) 6074–6076, https://doi.org/10.1021/ma020230t.

[8] O. Daugulis, A.H.R. Macarthur, F.C. Rix, J.L. Templeton, A Career in Catalysis: Maurice Brookhart, ACS Catal. 6 (2016) 1518–1532, https://doi.org/10.1021/acscatal.5b02216.

[9] D.A. Evans, L.M. Lee, I. Vargas-Baca, A.H. Cowley, Photophysical tuning of the aggregation-induced emission of a series of para-substituted aryl bis(imino) acenaphthene zinc complexes, Dalton Trans. 44 (2015) 11984–11996, https://doi.org/10.1039/C5DT01529D.

[10] V. Rosa, T. Avilés, G. Aullon, B. Covelo, C. Lodeiro, A new bis(1-naphthylimino) acenaphthene compound and its Pd(II) and Zn(II) complexes: Synthesis, characterization, solid-state structures and density functional theory studies on the syn and anti isomers, Inorg. Chem. 47 (2008) 7734–7744, https://doi.org/10.1021/ic800790u.

[11] D.N. Coventry, A.S. Batsanov, A.E. Goeta, J.A.K. Howard, T.B. Marder, Synthesis and molecular structures of α-diimines and their zinc and palladium dichloride complexes, Polyhedron. 23 (2004) 2789–2795, https://doi.org/10.1016/j.poly.2004.06.023.

[12] L.A. Brown, F.S. Wekesa, D.K. Unruh, M. Findlater, B.K. Long, BIAN-Fe(η6-C6H6): Synthesis, characterization, and l-lactide polymerization, J. Polym. Sci. Part A Polym. Chem. 55 (2017) 2824–2830, https://doi.org/10.1002/pola.28688.

[13] V.V. Khrizanforova, V.I. Morozov, M.N. Khrizanforov, A.N. Lukoyanov, O. N. Kataeva, I.L. Fedushkin, Y.H. Budnikova, Iron complexes of BIANs: Redox trends and electrocatalysis of hydrogen evolution, Polyhedron. 154 (2018) 77–82, https://doi.org/10.1016/j.poly.2018.07.041.

[14] F.S. Wekesa, R. Arias-Ugarte, L. Kong, Z. Sumner, G.P. McGovern, M. Findlater, Iron-Catalyzed Hydrosilylation of Aldehydes and Ketones under Solvent-Free Conditions, Organometallics. 34 (2015) 5051–5056, https://doi.org/10.1021/acs.organomet.5b00630.

[15] M.J. Supej, A. Volkov, L. Darko, R.A. West, J.M. Darmon, C.E. Schulz, K. A. Wheeler, H.M. Hoyt, Aryl-substituted BIAN complexes of iron dibromide: Synthesis, X-ray and electronic structure, and catalytic hydrosilylation activity, Polyhedron. 114 (2016) 403–414, https://doi.org/10.1016/j.poly.2016.02.020.

[16] K.M. Clark, J. Bendix, A.F. Heyduk, J.W. Ziller, Synthesis and characterization of a neutral titanium tris(iminosemiquinone) complex featuring redox-active ligands, Inorg. Chem. 51 (2012) 7457–7459, https://doi.org/10.1021/ic301059p.

[17] A.G. Morozov, I.L. Fedushkin, E. Irran, A. Grohmann, Titanium(IV) complexes supported by a dianionic acenaphthenediimine ligand: X-ray and spectroscopic studies of the metal coordination sphere, Inorg. Chem. Commun. 95 (2018) 50–55, https://doi.org/10.1016/j.inoche.2018.07.006.

[18] J. Bendix, K.M. Clark, Delocalization and Valence Tautomerism in Vanadium Tris (iminosemiquinone) Complexes, Angew. Chem Int. Ed. 55 (2016) 2748–2752, https://doi.org/10.1002/anie.201510403.

[19] V.G. Koshechko, V.E. Titov, V.N. Bondarenko, V.D. Pokhodenko, Electrochemical carboxylation of fluorocontaining imines with preparation of fluorinated N-phenylphenylglycines, J. Fluor. Chem. 129 (2008) 701–706, https://doi.org/10.1016/j.jfluchem.2008.06.010.

[20] M. Dunwell, Y. Yan, B. Xu, Understanding the influence of the electrochemical double-layer on heterogeneous electrochemical reactions, Curr. Opin. Chem. Eng. 20 (2018) 151–158, https://doi.org/10.1016/j.coche.2018.05.003.

[21] E. Kianfar, U. Monkowius, E. Portenkirchner, G. Knör, Synthesis and characterization of novel Re(BIAN) (CO)3Cl derivatives including the first example of a water-soluble tricarbonyl rhenium(I) complex with Bis(imino)acenaphthene ligands, Zeitschrift Fur Naturforsch. - Sect. B, J. Chem. Sci. 69 (2014) 691–698, https://doi.org/10.5560/ZNB.2014-4016.

[22] N.F. Romashev, A.L. Gushchin, I.S. Fomenko, P.A. Abramov, I. V. Mirzaeva, N.B. Kompan'kov, D.B. Kal'nyi, M.N. Sokolov, A new organometallic rhodium(I) complex with dpp-bian ligand: Synthesis, structure and redox behaviour, Polyhedron. 173 (2019) 114110. 10.1016/j.poly.2019.114110.

[23] A.L. Gushchin, N.F. Romashev, A.A. Shmakova, P.A. Abramov, M.R. Ryzhikov, I. S. Fomenko, M.N. Sokolov, Novel redox active rhodium(iii) complex with bis (arylimino)acenaphthene ligand: synthesis, structure and electrochemical studies, Mendeleev Commun. 30 (2020) 81–83, https://doi.org/10.1016/j.mencom.2020.01.027.

[24] J.G. Donkervoort, M. Bühl, J.M. Ernsting, C.J. Elsevier, Steric and electronic effects on the 103Rh NMR chemical shifts of Rh1(cyclooctadiene) compounds bearing N-donor ligands, Eur. J. Inorg. Chem. 1999 (1999) 27–33, https://doi.org/10.1002/(sici)1099-0682(199901)1999:1<27::aid-ejic27>3.0.co;2-4.

[25] H. Van Der Poel, G. Van Koten, K. Vrieze, Syntheses and NMR studies of five-co-ordinate rhodium(I) complexes with α-diimines (RNC(H)C(H)NR): [RhCl(CO)(η2-C2H4)(α-diimine)] and [RhCl(L)2(α-diimine)] (R = t-Bu, EtMe2C-; L = CO, PF3), Inorganica Chim. Acta. 51 (1981) 241–252, https://doi.org/10.1016/S0020-1693(00)88344-9.

[26] S.L. Rumble, The Synthesis of Amines and Imines Using Organometallic Catalysts, University of New South Wales, 2005.

[27] S.L. Rumble, M.J. Page, L.D. Field, B.A. Messerle, In situ catalysts for the intramolecular hydroamination of aminoalkynes - What ligand properties determine catalyst activity? Eur. J. Inorg. Chem. 2012 (2012) 2226–2231, https://doi.org/10.1002/ejic.201101307.

[28] E. Portenkirchner, E. Kianfar, N.S. Sariciftci, G. Knör, Two-electron carbon dioxide reduction catalyzed by rhenium(I) bis(imino)acenaphthene carbonyl complexes, ChemSusChem. 7 (2014) 1347–1351, https://doi.org/10.1002/cssc.201301116.

[29] N.J. Hill, I. Vargas-Baca, A.H. Cowley, Recent developments in the coordination chemistry of bis(imino)acenaphthene (BIAN) ligands with s- and p-block elements, Dalton Trans. 38 (2009) 240–253, https://doi.org/10.1039/B815079F.

[30] G. Giordano, R.H. Crabtree, R.M. Heintz, D. Forster, D.E. Morris, Di-μ-Chloro-Bis(η 4 -1,5-Cyclooctadiene)-Dirhodium(I), in: D.F. Shriver (Ed.), Inorganic Syntheses, 19th ed., 1979: pp. 88–90. 10.1002/9780470132593.ch22.

[31] J. Choudhury, S. Podder, S. Roy, Cooperative Friedel-Crafts catalysis in heterobimetallic regime: Alkylation of aromatics by π-activated alcohols, J. Am. Chem. Soc. 127 (2005) 6162–6163, https://doi.org/10.1021/ja0506004.

[32] A. Paulovicova, U. El-Ayaan, K. Shibayama, T. Morita, Y. Fukuda, Mixed-Ligand Copper(II) Complexes with the Rigid Bidentate Bis(N-arylimino)acenaphthene Ligand: Synthesis, Spectroscopic-, and X-ray Structural Characterization, Eur. J. Inorg. Chem. 2001 (2001) 2641–2646, https://doi.org/10.1002/1099-0682(200109)2001:10<2641::AID-EJIC2641>3.0.CO;2-C.

[33] M. Gasperini, F. Ragaini, S. Cenini, Synthesis of Ar-BIAN Ligands (Ar-BIAN = Bis (aryl)acenaphthenequinonediimine) Having Strong Electron-Withdrawing Substituents on the Aryl Rings and Their Relative Coordination Strength toward Palladium(0) and -(II) Complexes, Organometallics. 21 (2002) 2950–2957, https://doi.org/10.1021/om020147u.

[34] APEX3 (including SAINT and SADABS), Bruker AXS Inc., Madison, WI, (2016).

[35] Rigaku Oxford Diffraction, CrysAlisPro Software system, (2018).

[36] G.M. Sheldrick, SHELXT – Integrated space-group and crystal-structure determination, Acta Crystallogr. Sect. A Found. Adv. 71 (2015) 3–8, https://doi.org/10.1107/S2053273314026370.

[37] G.M. Sheldrick, Crystal structure refinement with SHELXL, Acta Crystallogr. Sect. C, Struct. Chem. 71 (2015) 3–8, https://doi.org/10.1107/S2053229614024218.

[38] M.J. Frisch, G.W. Trucks, H.B. Schlegel, G.E. Scuseria, M.A. Robb, J.R. Cheeseman, G. Scalmani, V. Barone, G.A. Petersson, H. Nakatsuji, X. Li, M. Caricato, A. V. Marenich, J. Bloino, B.G. Janesko, R. Gomperts, B. Mennucci, H.P. Hratchian, J. V. Ortiz, A.F. Izmaylov, J.L. Sonnenberg, D. Williams-Young, F. Ding, F. Lipparini, F. Egidi, J. Goings, B. Peng, A. Petrone, T. Henderson, D. Ranasinghe, V. G. Zakrzewski, J. Gao, N. Rega, G. Zheng, W. Liang, M. Hada, M. Ehara, K. Toyota, R. Fukuda, J. Hasegawa, M. Ishida, T. Nakajima, Y. Honda, O. Kitao, H. Nakai, T. Vreven, K. Throssell, J.A. Montgomery Jr., J.E. Peralta, F. Ogliaro, M. J. Bearpark, J.J. Heyd, E.N. Brothers, K.N. Kudin, V.N. Staroverov, T.A. Keith, R. Kobayashi, J. Normand, K. Raghavachari, A.P. Rendell, J.C. Burant, S.S. Iyengar, J. Tomasi, M. Cossi, J.M. Millam, M. Klene, C. Adamo, R. Cammi, J.W. Ochterski, R.L. Martin, K. Morokuma, O. Farkas, J.B. Foresman, D.J. Fox, Gaussian 16, Revision B.01 (2016).

[39] A.D. Becke, Density-functional thermochemistry. III. The role of exact exchange, J. Chem. Phys. 98 (1993) 5648–5652, https://doi.org/10.1063/1.464913.

[40] C. Lee, W. Yang, R.G. Parr, Development of the Colle-Salvetti correlation-energy formula into a functional of the electron density, Phys. Rev. B. 37 (1988) 785–789, https://doi.org/10.1103/PhysRevB.37.785.

[41] F. Weigend, R. Ahlrichs, Balanced basis sets of split valence, triple zeta valence and quadruple zeta valence quality for H to Rn: Design and assessment of accuracy, Phys. Chem. Chem. Phys. 7 (2005) 3297–3305, https://doi.org/10.1039/b508541a.

[42] M. Steinmetz, S. Grimme, Benchmark study of the performance of density functional theory for bond activations with (Ni, Pd)-based transition-metal catalysts, ChemistryOpen. 2 (2013) 115–124, https://doi.org/10.1002/open.201300012.

[43] S. Grimme, J. Antony, S. Ehrlich, H. Krieg, A consistent and accurate ab initio parametrization of density functional dispersion correction (DFT-D) for the 94

elements H-Pu, J. Chem. Phys. 132 (2010), 154104, https://doi.org/10.1063/1.3382344.
[44] M. Cossi, N. Rega, G. Scalmani, V. Barone, Energies, structures, and electronic properties of molecules in solution with the C-PCM solvation model, J. Comput. Chem. 24 (2003) 669–681, https://doi.org/10.1002/jcc.10189.
[45] V. Barone, M. Cossi, Quantum calculation of molecular energies and energy gradients in solution by a conductor solvent model, J. Phys. Chem. A. 102 (1998) 1995–2001, https://doi.org/10.1021/jp9716997.
[46] P. De Frémont, H. Clavier, V. Rosa, T. Avilés, P. Braunstein, Synthesis, characterization, and reactivity of cationic gold(I) α-diimine complexes, Organometallics. 30 (2011) 2241–2251, https://doi.org/10.1021/om2000426.
[47] R.A. Klein, C.J. Elsevier, F. Hartl, Redox Properties of Zerovalent Palladium Complexes Containing α-Diimine and p -Quinone Ligands, Organometallics. 16 (1997) 1284–1291, https://doi.org/10.1021/om960809d.
[48] S. Kannan, A.J. James, P.R. Sharp, Dinuclear diimine palladium(II) and platinum (II) hydroxo and amido complexes: Synthesis and X-ray crystal structures, Polyhedron. 19 (2000) 155–163, https://doi.org/10.1016/S0277-5387(99)00338-1.
[49] C. Fliedel, V. Rosa, C.I.M. Santos, P.J. Gonzalez, R.M. Almeida, C.S.B. Gomes, P. T. Gomes, M.A.N.D.A. Lemos, G. Aullón, R. Welter, T. Avilés, Copper(ii) complexes of bis(aryl-imino)acenaphthene ligands: Synthesis, structure, DFT studies and evaluation in reverse ATRP of styrene, Dalton Trans. 43 (2014) 13041–13054, https://doi.org/10.1039/c4dt01069h.
[50] C.J. Adams, N. Fey, J.A. Weinstein, Near-Infrared Luminescence from Platinum(II) Diimine Compounds, Inorg. Chem. 45 (2006) 6105–6107, https://doi.org/10.1021/ic060399d.
[51] R. van Asselt, C.J. Elsevier, Palladium complexes containing rigid bidentate nitrogen ligands as catalysts for carbon-carbon bond formation, Tetrahedron. 50 (1994) 323–334, https://doi.org/10.1016/S0040-4020(01)80757-2.
[52] D.S. Yambulatov, S.A. Nikolaevskii, M.A. Kiskin, T. V. Magdesieva, O.A. Levitskiy, D. V. Korchagin, N.N. Efimov, P.N. Vasil'ev, A.S. Goloveshkin, A.A. Sidorov, I.L. Eremenko, Complexes of Cobalt(II) Iodide with Pyridine and Redox Active 1,2-Bis (arylimino)acenaphthene: Synthesis, Structure, Electrochemical, and Single Ion Magnet Properties, Molecules. 25 (2020) 2054. 10.3390/molecules25092054.
[53] L. Yang, D.R. Powell, R.P. Houser, Structural variation in copper(I) complexes with pyridylmethylamide ligands: Structural analysis with a new four-coordinate geometry index, τ4, Dalton Trans. 36 (2007) 955–964, https://doi.org/10.1039/b617136b.
[54] A.W. Addison, T.N. Rao, J. Reedijk, J. Van Rijn, G.C. Verschoor, Synthesis, structure, and spectroscopic properties of copper(II) compounds containing nitrogen-sulphur donor ligands; the crystal and molecular structure of aqua[1,7-bis (N-methylbenzimidazol-2′;-yl)-2,6-dithiaheptane]copper(II) perchlorate, Dalton Trans. 1984 (1984) 1349–1356, https://doi.org/10.1039/DT9840001349.
[55] J. Li, Z. Tian, Z. Xu, S. Zhang, Y. Feng, L. Zhang, Z. Liu, Highly potent half-sandwich iridium and ruthenium complexes as lysosome-targeted imaging and anticancer agents, Dalton Trans. 47 (2018) 15772–15782, https://doi.org/10.1039/C8DT02963F.
[56] D. Sieh, J. Schöffel, P. Burger, Synthesis of a chloro protected iridium nitrido complex, Dalton Trans. 40 (2011) 9512, https://doi.org/10.1039/c1dt10886g.
[57] Z. Wang, S.M. Lu, J. Li, J. Wang, C. Li, Unprecedentedly High Formic Acid Dehydrogenation Activity on an Iridium Complex with an N, N′-Diimine Ligand in Water, Chem. Eur. J. 21 (2015) 12592–12595, https://doi.org/10.1002/chem.201502086.
[58] S.A. Bezman, P.H. Bird, A.R. Fraser, J.A. Osborn, Metallacyclic Complexes of Iridium, Inorg. Chem. 19 (1980) 3755–3763, https://doi.org/10.1021/ic50214a035.
[59] S. Gonell, M. Poyatos, E. Peris, Pyrene-based bisazolium salts: From luminescence properties to Janus-type bis-N-heterocyclic carbenes, Chem. Eur. J. 20 (2014) 9716–9724, https://doi.org/10.1002/chem.201304952.
[60] A. Petronilho, M. Rahman, J.A. Woods, H. Al-Sayyed, H. Müller-Bunz, J.M. Don MacElroy, S. Bernhard, M. Albrecht, Photolytic water oxidation catalyzed by a molecular carbene iridium complex, Dalton Trans. 41 (2012) 13074, https://doi.org/10.1039/c2dt30403a.
[61] K.F. Donnelly, R. Lalrempuia, H. Müller-Bunz, M. Albrecht, Regioselective electrophilic C-H bond activation in triazolylidene metal complexes containing a N-bound phenyl substituent, Organometallics. 31 (2012) 8414–8419, https://doi.org/10.1021/om300983m.
[62] K.V. Vasudevan, R.R. Butorac, C.D. Abernethy, A.H. Cowley, Synthesis and coordination compounds of a bis(imino)acenaphthene (BIAN)-supported N-heterocyclic carbene, Dalton Trans. 39 (2010) 7401, https://doi.org/10.1039/c0dt00278j.
[63] M.M. Khusniyarov, K. Harms, O. Burghaus, J. Sundermeyer, Molecular and Electronic Structures of Homoleptic Nickel and Cobalt Complexes with Non-Innocent Bulky Diimine Ligands Derived from Fluorinated 1,4-Diaza-1,3-butadiene (DAD) and Bis(arylimino)acenaphthene (BIAN), Eur. J. Inorg. Chem. 2006 (2006) 2985–2996, https://doi.org/10.1002/ejic.200600236.
[64] I.L. Fedushkin, A.A. Skatova, V.A. Chudakova, G.K. Fukin, Four-step reduction of dpp-bian with sodium metal: Crystal structures of the sodium salts of the mono-, di-, tri- and tetraanions of dpp-bian, Angew. Chem Int. Ed. 42 (2003) 3294–3298, https://doi.org/10.1002/anie.200351408.
[65] P.J. Larson, F.S. Wekesa, A. Singh, C.R. Smith, A. Rajput, G.P. McGovern, D. K. Unruh, A.F. Cozzolino, M. Findlater, Synthesis, characterization, electrochemical properties and theoretical calculations of (BIAN) iron complexes, Polyhedron. 159 (2019) 365–374, https://doi.org/10.1016/j.poly.2018.11.060.
[66] K. Vasudevan, A.H. Cowley, Synthesis and structures of 1,2-bis(imino)acenaphthene (BIAN) lanthanide complexes that involve the transfer of zero, one, or two electrons, Chem. Commun. 2007 (2007) 3464–3466, https://doi.org/10.1039/b708758f.
[67] G. Reeske, C.R. Hoberg, N.J. Hill, A.H. Cowley, Capture of phosphorus(I) and arsenic(I) moieties by a 1,2-bis(arylimino) acenaphthene (aryl-BIAN) ligand. A case of intramolecular charge transfer, J. Am. Chem. Soc. 128 (2006) 2800–2801, https://doi.org/10.1021/ja058459m.
[68] T. Mahabiersing, H. Luytenn, R.C. Nieuwendam, F. Hartl, Synthesis, spectroscopy and spectroelectrochemistry of chlorocarbonyl {1,2-bis[(2,6-diisopropylphenyl) imino]-acenaphthene-κ2-N, N′}rhodium(I), Collect. Czechoslov. Chem. Commun. 68 (2003) 1687–1709, https://doi.org/10.1135/cccc20031687.
[69] A. Singha Hazari, R. Ray, M.A. Hoque, G.K. Lahiri, Electronic Structure and Multicatalytic Features of Redox-Active Bis(arylimino)acenaphthene (BIAN)-Derived Ruthenium Complexes, Inorg. Chem. 55 (2016) 8160–8173, https://doi.org/10.1021/acs.inorgchem.6b01280.
[70] C.J. Allan, B.F.T. Cooper, H.J. Cowley, J.M. Rawson, C.L.B. Macdonald, Non-innocent ligand effects on low-oxidation-state indium complexes, Chem. Eur. J. 19 (2013) 14470–14483, https://doi.org/10.1002/chem.201301881.
[71] P.A. Abramov, A.A. Dmitriev, K.V. Kholin, N.P. Gritsan, M.K. Kadirov, A. L. Gushchin, M.N. Sokolov, Mechanistic study of the [(dpp-bian)Re(CO)3Br] electrochemical reduction using in situ EPR spectroscopy and computational chemistry, Electrochim. Acta. 270 (2018) 526–534, https://doi.org/10.1016/j.electacta.2018.03.111.
[72] O.M. Williams, A.H. Cowley, M.J. Rose, Structural and electronic characterization of multi-electron reduced naphthalene (BIAN) cobaloximes, Dalton Trans. 44 (2015) 13017–13029, https://doi.org/10.1039/C5DT00924C.
[73] A.S. Hazari, A. Das, R. Ray, H. Agarwala, S. Maji, S.M. Mobin, G.K. Lahiri, Tunable Electrochemical and Catalytic Features of BIAN- and BIAO-Derived Ruthenium Complexes, Inorg. Chem. 54 (2015) 4998–5012, https://doi.org/10.1021/acs.inorgchem.5b00615.
[74] P. Mondal, H. Agarwala, R.D. Jana, S. Plebst, A. Grupp, F. Ehret, S.M. Mobin, W. Kaim, G.K. Lahiri, Sensitivity of a strained C-C single bond to charge transfer: Redox activity in mononuclear and dinuclear ruthenium complexes of bis (arylimino)acenaphthene (BIAN) ligands, Inorg. Chem. 53 (2014) 7389–7403, https://doi.org/10.1021/ic500730m.
[75] N. Elgrishi, M.B. Chambers, X. Wang, M. Fontecave, Molecular polypyridine-based metal complexes as catalysts for the reduction of CO2, Chem. Soc. Rev. 46 (2017) 761–796, https://doi.org/10.1039/c5cs00391a.
[76] K. Elouarzaki, V. Kannan, V. Jose, H.S. Sabharwal, J. Lee, Recent Trends, Benchmarking, and Challenges of Electrochemical Reduction of CO 2 by Molecular Catalysts, Adv. Energy Mater. 9 (2019) 1900090, https://doi.org/10.1002/aenm.201900090.
[77] R. Francke, B. Schille, M. Roemelt, Homogeneously Catalyzed Electroreduction of Carbon Dioxide - Methods, Mechanisms, and Catalysts, Chem. Rev. 118 (2018) 4631–4701, https://doi.org/10.1021/acs.chemrev.7b00459.
[78] M.V. Vollmer, C.W. Machan, M.L. Clark, W.E. Antholine, J. Agarwal, H.F. Schaefer, C.P. Kubiak, J.R. Walensky, Synthesis, spectroscopy, and electrochemistry of (α-diimine)M(CO)3Br, M = Mn, Re, complexes: Ligands isoelectronic to bipyridyl show differences in CO2 reduction, Organometallics. 34 (2015) 3–12, https://doi.org/10.1021/om500838z.
[79] W. Yin, A. Grimaud, I. Azcarate, C. Yang, J.M. Tarascon, Electrochemical Reduction of CO2 Mediated by Quinone Derivatives: Implication for Li-CO2 Battery, J. Phys. Chem. C. 122 (2018) 6546–6554, https://doi.org/10.1021/acs.jpcc.8b00109.
[80] J.P. Collin, J.P. Sauvage, Electrochemical reduction of carbon dioxide mediated by molecular catalysts, Coord. Chem. Rev. 93 (1989) 245–268, https://doi.org/10.1016/0010-8545(89)80018-9.
[81] D. Krisch, H. Sun, K. Pellumbi, K. Faust, U.-P. Apfel, W. Schöfberger, Tuning the Electronic Properties of Homoleptic Silver(I) bis-BIAN Complexes towards Efficient Electrocatalytic CO2 Reduction, Catalysts. 12 (2022) 545, https://doi.org/10.3390/catal12050545.
[82] M. Aresta, A. Dibenedetto, E. Quaranta (Eds.), Reaction Mechanisms in Carbon Dioxide Conversion, Springer Berlin Heidelberg, Berlin, Heidelberg, 2016.
[83] J.Y. Becker, B. Vainas, R. Eger, L. Kaufman, Electrocatalytic reduction of CO2 to oxalate by Ag“ and Pd” porphyrins, Chem. Commun. 1985 (1985) 1471–1472, https://doi.org/10.1039/C39850001471.
[84] S.S. Gayathri, A. Patnaik, Electrical rectification from a fullerene[60]-dyad based metal–organic–metal junction, Chem. Commun. 2006 (2006) 1977–1979, https://doi.org/10.1039/B602203K.
[85] S.S. Gayathri, A. Patnaik, A new fullerene C60-didodecyloxy benzene dyad: An evidence for ground state electron transfer, Chem. Phys. Lett. 414 (2005) 198–203, https://doi.org/10.1016/j.cplett.2005.08.043.